Available online at www.sciencedirect.com
SCIENCE DIRECT®
Biochemical Pharmacology 66 (2003) 1915–1924
Biochemical Pharmacology
www.elsevier.com/locate/biochempharm

Effects of Li^+ transport and Li^+ immobilization on Li^+/Mg^{2+} competition in cells: implications for bipolar disorder

Brian T. Layden[a], Abde M. Abukhdeir[a], Nicole Williams[a], Carla P. Fonseca[b], Laura Carroll[a], Margarita M.C.A. Castro[b], Carlos F.G.C. Geraldes[b], Fred B. Bryant[c], Duarte Mota de Freitas[a,*]

[a]*Department of Chemistry, Loyola University Chicago, 6525 N. Sheridan Rd., Chicago, IL 60626, USA*
[b]*Department of Biochemistry and Center for Neurosciences, University of Coimbra, Pólo I/Praça Marquês de Pombal, 3000 Coimbra, Portugal*
[c]*Department of Psychology, Loyola University Chicago, 6525 N. Sheridan Rd., Chicago, IL 60626, USA*

Received 13 May 2003; accepted 7 July 2003

Abstract

Li^+/Mg^{2+} competition has been implicated in the therapeutic action of Li^+ treatment in bipolar illness. We hypothesized that this competition depended on cell-specific properties. To test this hypothesis, we determined the degree of Li^+ transport, immobilization, and Li^+/Mg^{2+} competition in lymphoblastomas, neuroblastomas, and erythrocytes. During a 50 mmol/L Li^+-loading incubation, Li^+ accumulation at 30 min (mmoles Li^+/L cells) was the greatest in lymphoblastomas (11.1 ± 0.3), followed by neuroblastomas (9.3 ± 0.5), and then erythrocytes (4.0 ± 0.5). Li^+ binding affinities to the plasma membrane in all three cell types were of the same order of magnitude; however, Li^+ immobilization in intact cells was greatest in neuroblastomas and least in erythrocytes. When cells were loaded for 30 min in a 50 mmol/L Li^+-containing medium, the percentage increase in free intracellular $[Mg^{2+}]$ in neuroblastoma and lymphoblastoma cells (~55 and ~52%, respectively) was similar, but erythrocytes did not exhibit any substantial increase (~6%). With the intracellular $[Li^+]$ at 15 mmol/L, the free intracellular $[Mg^{2+}]$ increased by the greatest amount in neuroblastomas (~158%), followed by lymphoblastomas (~75%), and then erythrocytes (~50%). We conclude that Li^+ immobilization and transport are related to free intracellular $[Mg^{2+}]$ and to the extent of Li^+/Mg^{2+} competition in a cell-specific manner.

Keywords: Fluorescence; NMR; Atomic absorption; Neuroblastoma; Lymphoblastoma

1. Introduction

Elucidation of the therapeutic effect(s) of Li^+ treatment will provide insight into the biochemical abnormality present in bipolar disorder. Because Li^+ and Mg^{2+} have similar ionic potentials, Li^+ was proposed to compete with Mg^{2+} for Mg^{2+} binding sites in biomolecules [1]. Evidence for this ionic competition has been observed with nucleotides [2], PMs [3], and human RBCs [4]. It has also been demonstrated that Li^+/Mg^{2+} competition can occur in human neuroblastoma cells [5], a nerve cell model, even at therapeutic $[Li^+]_i$ levels after chronic Li^+ treatment, where the percentage increase in $[Mg^{2+}]_f$ was between 11 and 37% [6]. These increases are small; however, larger increases in $[Mg^{2+}]_f$ would be toxic to cells [7], and are not required to have a significant effect on the activity of signal-transduction processes [8,9]. It is necessary to determine the dependence of Li^+/Mg^{2+} competition on the kinetic and thermodynamic properties of $[Li^+]_i$, because these properties are known to vary among different cell types [10].

* Corresponding author. Tel.: +1-773-508-3091; fax: +1-773-508-3086.
E-mail address: dfreita@luc.edu (D.M.d. Freitas).

Abbreviations: AA, atomic absorption; cP, centipoise; DIDS, 4,4′-diisothiocynostilbene-2,2′-disulfonic acid; HBS, HEPES-buffered saline; HMA, 5-(*N*,*N*′-hexamethylene)-amiloride; $HTmDOTP^{4-}$, thulium(III) 1,4,7,10-tetraazacyclododecane-*N*,*N*′,*N*″,*N*‴-tetramethylenephosphonate; k_{in} and k_{out}, rate constants of Li^+ influx and efflux, respectively; K_{Li}, lithium binding constant; $[Li^+]_i$, total intracellular Li^+ concentration; $[Li^+]_{ex}$, total extracellular Li^+ concentration; $[Mg^{2+}]_f$, free intracellular Mg^{2+} concentration; MRI, magnetic resonance imaging; PBS, phosphate-buffered solution; PM, plasma membrane; RBCs, red blood cells; T_1, spin–lattice relaxation time; T_2, spin–spin relaxation time; τ_c, correlation time; v_{in} and v_{out}, initial rate constants of Li^+ influx and efflux, respectively.

0006-2952/$ – see front matter © 2003 Elsevier Inc. All rights reserved.
doi:10.1016/j.bcp.2003.07.001

Specific sites of enzyme inhibition by Li^+ have been proposed for inositol monophosphatase [11], glycogen synthase kinase-3β [12–14], adenylate cyclase [15], and guanine–nucleotide binding proteins [9], in which each of the proteins is Mg^{2+}-dependent. Li^+/Mg^{2+} competition may therefore be the underlying theme in these more specific hypothesized mechanisms. It is important to elucidate how this competition varies among different cell types, because this may influence Li^+ inhibition of these specific site(s) of action. For example, Li^+ has been observed to exhibit different kinds of regulation of adenylate cyclase in two cell types: Li^+ inhibition of adenylate cyclase, under therapeutic conditions, is observed in urinary epithelia [16], whereas in adipose cells, Li^+ inhibition does not occur [17]. The Li^+/Mg^{2+} competition observed within the cell may affect these enzymes, and it is important to ascertain which cell types will be affected the most by Li^+ through the Li^+/Mg^{2+} competition mechanism.

Because this ionic competition may potentially explain the therapeutic action of Li^+ in the treatment of bipolar illness, a better understanding of this mechanism may lead to the development of less toxic drugs in its treatment. In this study, we demonstrate in lymphoblastoma, neuroblastoma, and RBCs that the extent of Li^+/Mg^{2+} competition depends on the cell-type specific properties of Li^+ transport and immobilization.

2. Materials and methods

2.1. Materials

Furaptra was purchased from Molecular Probes, and the shift reagent, $HTmDOTP^{4-}$ as a sodium salt, was obtained from Macrocyclics. All other biochemicals were purchased from Sigma Chemical Co. The human lymphoblastoma CCRF-CEM cell line was purchased from the American Type Culture Collection (ATCC). The human neuroblastoma SH-SY5Y cell line was provided by Dr. E. Stubbs, Jr. (Department of Neurology, Loyola University Chicago). Human RBCs were purchased from the Life Source blood bank.

2.2. Characterization of Li^+ transport pathways in lymphoblastoma cells

The lymphoblastoma CCRF-CEM cells were grown as recommended by the ATCC. For both Li^+-influx and -efflux experiments, the cells were harvested and washed once in PBS (1090 *g*/5 min/4°). In order to test which pathway was involved in Li^+ transport, we supplemented the growth medium with one of the following transport inhibitors: 0.10 mmol/L ouabain, 0.05 mmol/L DIDS, 0.10 mmol/L bumetanide, 0.10 mmol/L phloretin, and 0.10 mmol/L HMA, which inhibit Na^+/K^+–ATPase, anion exchange, Na^+–K^+–Cl^- cotransport, and Na^+–Li^+ countertransport (for both phloretin and HMA) pathways, respectively [10,18]. The Na^+ channel activator, veratridine (at 0.50 mmol/L), was also tested in these transport experiments [10].

For Li^+ influx experiments, cells were incubated (1–5% cytocrit) in RPMI-1640 growth medium containing 20 mmol/L LiCl and supplemented with or without one of the transport modulators. Aliquots of the Li^+-loaded cells were washed twice in ice-cold choline-PBS (958 *g*/1 min/4°) [19] after the following Li^+-loading times: 5, 10, 20, 30, 40, 50, 60, 80, 100, 120, and 150 min. Pelleted cells were lysed and measured by AA spectrophotometry [19].

For Li^+ efflux experiments, the cells were incubated (1–5% cytocrit) with 110 mmol/L LiCl-containing PBS for 30 min [5], and then washed twice with ice-cold choline-PBS before the addition of Li^+-free RPMI-1640 growth medium (1–5% cytocrit) in the absence or presence of the aforementioned ion channel modulators. Li^+ efflux was measured in aliquots of this RPMI-1640 cell suspension, which were isolated and pelleted after the same periods as above, except that 0 min of Li^+ incubation was also measured in the efflux experiments. Pelleted cells were prepared as described [19].

For the influx experiments, the following equation was used:

$$[Li^+]_t = [Li^+]_\infty(1 - \exp^{(-k_{in})(t)}), \quad (1)$$

where k_{in} is the rate constant for Li^+ influx; and $[Li^+]_\infty$ and $[Li^+]_t$ are the $[Li^+]_i$ values when the transport has reached equilibrium or at the different times (t), respectively. Eq. (1) was fitted to a nonlinear one-phase exponential graph. For the efflux experiments, the following equation was used:

$$[Li^+]_t = [Li^+]_{max}\exp^{(-k_{out})(t)}. \quad (2)$$

To calculate k_{out} by AA spectrophotometry, we fitted Eq. (2) to a nonlinear one-phase exponential decay graph. $[Li^+]_{max}$ is the estimated $[Li^+]_i$ at time 0 for the efflux experiments. For v_{in} or v_{out} estimates, the first derivatives of Eqs. (1) and (2) at time 0 were used ($v_{(in\ or\ out)} = k_{(in\ or\ out)}[Li^+]_{(\infty\ or\ max)}$).

2.3. Comparison of Li^+ influx among cell types

Lymphoblastoma cells were prepared as described above. RBCs were prepared from whole blood by washing three times in PBS. The neuroblastoma cells were prepared as previously described [19]. Each cell type was incubated in 50 mmol/L LiCl-containing PBS with measurements at 15, 30, 45, and 60 min [5]. With each measurement, the cells were washed in ice-cold choline-PBS and lysed as previously described [19]. Cytocrits and hematocrits were between 1 and 5% for each transport experiment and were measured with an IEC model MB microhematofuge. We used a Perkin-Elmer AA spectrophotometer (AAnalyst 100) to determine $[Li^+]_i$, and dilution was taken into account.

2.4. Cell viability of agarose-embedded lymphoblastoma cells

For embedding of the cells in agarose threads, the cells were prepared as previously described [10,20] and perfused with RPMI-1640 growth medium. To determine cell viability, we monitored the intracellular pH via the observed ^{31}P NMR chemical shift separation between the resonances of the α- and γ-phosphates of ATP, which was calculated by extrapolation to previously published pH-dependent chemical shift values [21]. The intracellular ATP concentration was assessed by the ratio of the peak areas of the β-phosphate of ATP over P_i ([β-ATP]/[P_i]); this was a modification of a method in which the sum of each area of the ATP phosphate peaks over P_i was used [20]. These ^{31}P NMR experiments were performed on a Varian Unity-500 spectrometer (202.9 MHz) with 2400 transients, 60° pulses, a 0.998 s acquisition time with proton decoupling, 19,968 data points, 0.55 s delay time, 20 Hz line broadening, and a total accumulation time of 1 hr.

2.5. Li^+ binding and immobilization to plasma membranes and intact cells

For ^{7}Li NMR relaxation measurements, the agarose-embedded lymphoblastoma cells were perfused in 7 mmol/L LiCl-containing RPMI-1640 growth medium supplemented with 3 mmol/L $HTmDOTP^{4-}$ for 3 hr in order to resolve the intracellular ^{7}Li resonance [10]. Cell viability was determined at the conclusion of each experiment using the Trypan blue dye exclusion assay [22]. The $[Li^+]_i$ (in mmoles Li^+/L cells) values in lymphoblastoma cell suspensions were determined by AA spectrophotometry after 3 hr in 7 mmol/L LiCl-containing growth medium.

The lymphoblastoma [23], neuroblastoma [24], and RBC [25] PMs were prepared, and the final PM pellet was washed twice in 5 mmol/L Tris–Cl buffer (pH 7.3) and stored at −80.0° for less than 2 weeks before use. Because viscosity affects relaxation rates [26], the viscosity was adjusted to 5 cP with polyvinyl pyrrolidone (MW-360,000); 5 cP is a reasonable estimate of intracellular viscosity [27]. The viscosities were measured with a Brookfield Cone Plate viscometer. The protein concentration was determined by the method of Bradford [28].

^{7}Li NMR relaxation measurements were conducted on a Varian VXR-400S NMR spectrometer equipped with a multinuclear 10 mm broadband probe at 155.4 MHz. ^{7}Li NMR T_1 and T_2 relaxation measurements were determined using the inversion recovery and the Carr–Purcell–Meiboom–Gill pulse sequences [26], respectively. We used the ^{7}Li NMR T_1 values, obtained during a Li^+ titration, to determine K_{Li} to the PM fractions as previously described [26,29]. Each relaxation value was determined by use of seven delay values, with at least two transients per delay value, an acquisition time of 0.979 s, and 19,584 data points.

2.6. Interpretation of the [^{7}Li] NMR relaxation measurements

For qualitative assessment of the relaxation data, the physical meaning of the T_1, T_2, T_1/T_2, and τ_c (a scale of Li^+ motion) NMR parameters needs to be explained. When the τ_c value of ^{7}Li is short with respect to the NMR frequency, the ion is free, resulting in $T_1 \approx T_2$. When Li^+ binds, the value τ_c becomes greater than the NMR frequency, resulting in $T_1 > T_2$. Only one type of Li^+ binding site is generally assumed to be present, as well as mono-exponential relaxation of the ^{7}Li nucleus, and fast exchange of Li^+ between free and bound states [26]. These are reasonable assumptions, considering the lability and low association constants associated with Li^+ binding (even for a tridentate ligand-like ATP) [2,3], the lack of sensitivity of the chemical shift and relaxation times of the ^{7}Li nucleus to the type of coordinating atoms present in its binding site(s) and its small quadrupolar coupling constant relative to ^{23}Na [30], which lead to much longer relaxation times than for ^{23}Na. Based on these assumption, it can then be shown that T_{1obs} and T_{2obs} are given by the expressions [21,25,26]:

$$\left(\frac{1}{T_{1obs}}\right) \propto f_b\left(\frac{1}{T_{1b}}\right), \tag{3}$$

$$\left(\frac{1}{T_{2obs}}\right) \propto f_b\left(\frac{1}{T_{2b}}\right), \tag{4}$$

where f_b is the fraction of bound Li^+. The T_{1obs} and T_{2obs} values are each directly related to f_b and K_{Li}. The ratio of Eqs. (3) and (4) results in $(T_1/T_2)_{obs} \sim (T_1/T_2)_b$, which indicates that the T_1/T_2 ratio is independent of f_b, and therefore also independent of K_{Li}. Relaxation of the ^{7}Li nucleus is governed by a major dipolar contribution (T_{1dd} and T_{2dd}) as well as a small quadrupolar contribution of the ^{7}Li nucleus [26]. Assuming only a dipolar contribution, when the Li^+ immobilization is such that $\omega\tau_c \gg 1$, where ω is the Larmor frequency of ^{7}Li, the relaxation equations can be simplified [21]:

$$\left(\frac{1}{T_1}\right)_{dd} \propto \tau_c^{-1}, \tag{5}$$

$$\left(\frac{1}{T_2}\right)_{dd} \propto \tau_c. \tag{6}$$

This indicates that the dipolar contribution to the observed T_1 and T_2 relaxation values is directly and inversely proportional to τ_c, respectively. Furthermore, the ratio of these dipole–dipole relaxation values, $(T_1/T_2)_{dd}$, is directly proportional to τ_c^2, which makes this a sensitive measure of the degree of immobilization. The quadrupolar contribution to ^{7}Li relaxation, when $\omega\tau_c \gg 1$ [30–33], leads to the same conclusion: $(1/T_1)_q \propto q_{zz}\tau_c^{-1}$, $(1/T_2)_q \propto q_{zz}\tau_c$, so that $(T_1/T_2)_q \propto \tau_c^2$ (where q_{zz} is the electrical field gradient at the nucleus, which is assumed to have axial symmetry). Thus, in the present interpretation of ^{7}Li relaxation data, only one type of binding sites was considered, and the

T_1/T_2 ratio was used as a measure of correlation time and hence Li^+ immobilization (ratio of Eqs. (5) and (6)), which is independent of the fraction of bound Li^+ and Li^+ binding affinity (ratio of Eqs. (3) and (4)). We used the T_1 and T_2 values independently to examine f_b and hence Li^+ binding (Eqs. (3) and (4)). However, the correlation time has a direct effect on these values (Eqs. (5) and (6)).

Besides binding to a macromolecule, Li^+ may also bind to a small molecule like ATP, with a bound fraction f'_b, a rotational correlation time τ'_c, and an electrical field gradient q'_{zz}. Because of the very different molecular sizes of the macromolecule and ATP, τ'_c will be several orders of magnitude shorter than τ_c, leading to $\omega\tau'_c < 1$. In this extreme narrowing condition, Li^+–ATP binding will give dipolar and quadrupolar contributions to $(1/T_1)$ and $(1/T_2)$, which are proportional to τ'_c, but are negligible relative to the contributions from Li^+–macromolecule binding. In particular, the contribution of Li^+–ATP binding to $(1/T_2)_q$ ($\propto f'_b q'^2_{zz} \tau'_c$) is negligible relative to that from Li^+–macromolecule binding ($\propto f_b q^2_{zz} \tau_c$), because the two sites are expected to have much smaller differences of electric field gradients than of rotational correlation times, $(q'_{zz}/q_{zz}) \ll (\tau_c/\tau'_c)$.

Moreover, Li^+ binds only weakly and not extensively to a small molecule such as ATP, where K'_{Li} and f'_b are small [2,3]. Thus, even in the presence of Li^+ binding to small molecules like ATP, the relationship $(T_1/T_2)_{obs} \propto \tau_c^2$ is still maintained. This is because τ'_c of ATP-bound Li^+ does not increase much relative to that of free Li^+, and so it will not be appreciably immobilized [2,3]. In contrast, immobilization occurs for Li^+ ions bound to macromolecular components (i.e. τ_c will increase significantly) [3,26]. However, as opposed to ^{23}Na, the visibility of the ^7Li NMR resonance would be expected to be near 100%, since previous work has found Li^+ visibility to be close to 100% in RBC membrane suspensions [3,26] and in intact human neuroblastoma SH-SY5Y cells [10].

2.7. Li^+/Mg^{2+} competition by fluorescence and ^{31}P NMR spectroscopy

Previous work has validated the fluorescence and ^{31}P NMR methods for studying Li^+/Mg^{2+} competition and found that the fluorescence method was the most sensitive for cellular studies of changes in $[Mg^{2+}]_f$ [2,26]. In the present study, we used fluorescence spectroscopy to measure changes in $[Mg^{2+}]_f$ with lymphoblastoma and neuroblastoma cells, but for RBCs, the ^{31}P NMR method was used because of the strong intrinsic fluorescence of hemoglobin [4].

2.8. Li^+/Mg^{2+} competition in neuroblastoma and lymphoblastoma cells

The cells were loaded with 10 μmol/L furaptra as previously described [19], and incubated at 37° in either Li^+-free or 50 mmol/L LiCl-containing PBS; probenecid and $MnCl_2$ were used as previously described [5]. For the fluorescence method, $[Mg^{2+}]_f$ was determined on a PTI QuantaMaster QM-1 fluorimeter with the cuvette holder water-jacketed to 37°. The excitation spectrum of furaptra was scanned between 300 and 400 nm, with the emission set at 510 nm, and analyzed as a fluorescence intensity ratio (335/370). For the fluorescence experiments, $[Mg^{2+}]_f$ was calculated as previously described [2].

2.9. Li^+/Mg^{2+} competition in RBCs

RBCs were prepared by washing of whole blood three times with PBS and then suspension of cells at 50% hematocrit in PBS (Li^+-free) or at 1–5% hematocrit in either 50 mmol/L LiCl-containing PBS for 30 min or 150 mmol/L LiCl-containing HBS for 60 min [18]. The Li^+-loaded RBCs were centrifuged and resuspended at 50% hematocrit in the respective Li^+-containing buffer for the ^{31}P NMR measurements. For the ^{31}P NMR experiments, intracellular $[Mg^{2+}]_f$ was calculated as previously described [2]. Because the RBC experiments were performed under modified hematocrit conditions, we assessed whether the 30 min ^{31}P NMR measurement period affected the $[Li^+]_i$ in the RBCs for both Li^+ conditions.

The ^{31}P NMR experiments were performed on a Varian Unity-400S NMR spectrometer (161.9 MHz) with 1200 transients, a 60° pulse, 0.800 s acquisition time with proton decoupling, 16,000 data points, 0.5 s delay time, 20 Hz line broadening, and a total accumulation time of 26 min [10].

2.10. Statistical analyses

To test for statistical differences between pairs of means, we used independent sample *t*-tests. To test the statistical significance of hypothesized patterns of differences across multiple sample means, we used planned orthogonal between-group contrasts [34]. We used one-way ANOVA as a test of homogeneity in sample means across multiple experimental conditions that we did not expect to differ. We used a sequentially rejective Bonferroni-type procedure [35] to control for inflation in the Type I error rate when conducting multiple statistical comparisons.

3. Results

3.1. Li^+ transport pathways in lymphoblastoma cells

We investigated Li^+ influx and efflux in lymphoblastoma cells in the presence of different transport pathway modulators. We used orthogonal between-group contrasts to test the hypothesized pattern of mean differences in k_{in} and v_{in} values across the seven experimental conditions (control, veratidine, ouabain, DIDS, phloretin, HMA, and bumetadine), specifying *a priori* weights of 1, 1, −6, 1, 1,

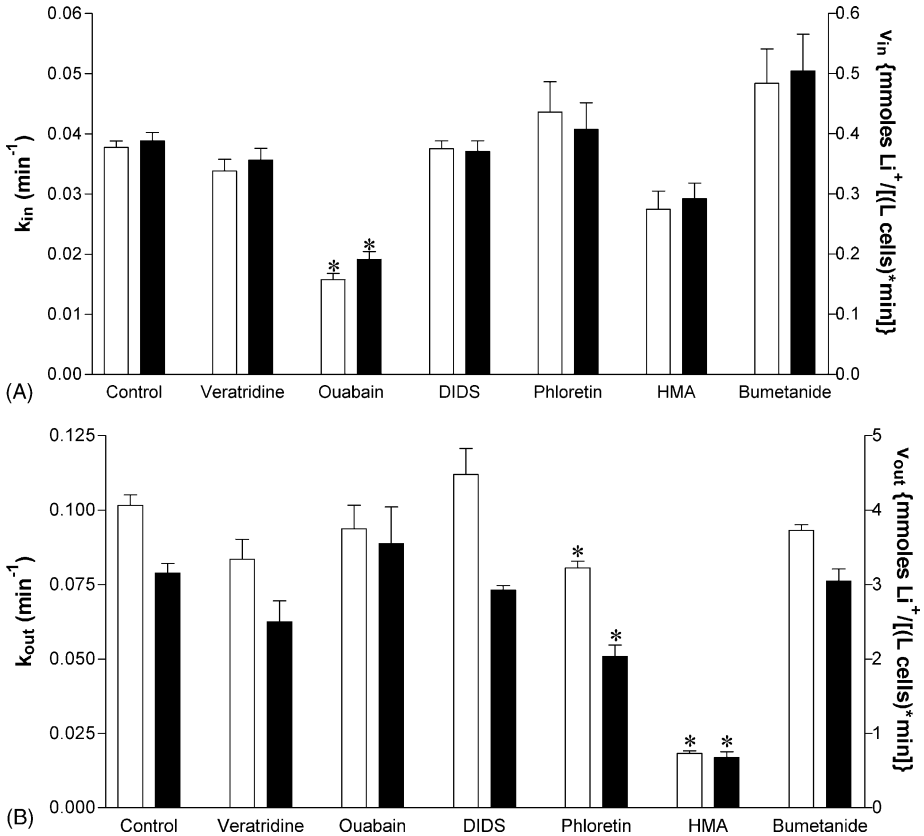

Fig. 1. Li^+ transport pathways in human lymphoblastoma CCRF-CEM cells. Li^+ influx (A) transport rates (k_{in}, white bars and v_{in}, black bars) and Li^+ efflux (B) transport rates (k_{out}, white bars and v_{out}, black bars) in the presence of modulators for the following pathways (modulators indicated in parentheses): voltage-sensitive Na^+ channels (veratridine), Na^+/K^+–ATPase (ouabain), anion exchange (DIDS), Na^+–Li^+ countertransport (phloretin and HMA), and Na^+–K^+–Cl^- cotransport (bumetanide) pathways in human lymphoblastoma cells. (*) Indicates a statistically significant effect ($P < 0.05$) compared to the control condition. For control experiments, $N > 20$, whereas for the experimental conditions, $N \geq 3$. Values represent means ± SEM. The left *y*-axes correspond to k_{in} or k_{out} (min^{-1}), and the right *y*-axes correspond to v_{in} or v_{out} (mmoles Li^+/L of cells).

1, and 1 for the means of the seven conditions, respectively (Fig. 1A). As hypothesized that ouabain inhibited Li^+ influx, the planned contrast was statistically significant for both k_{in} ($t(67) = 5.76$, one-tailed $P < 0.0001$), and v_{in} ($t(67) = 3.97$, one-tailed $P < 0.0001$), indicating that ouabain was the only modulator that produced a significant effect on Li^+ influx as compared to the control condition (Fig. 1A). These findings indicate that Na^+/K^+–ATPase is a major Li^+ influx pathway in lymphoblastoma cells.

We also used orthogonal between-group contrasts to test the hypothesized pattern of mean differences in k_{out} and v_{out} values across the seven experimental conditions (see above), specifying *a priori* weights of 2, 2, 2, 2, −5, −5, and 2 for the means of the seven conditions, respectively (Fig. 1B). As hypothesized that HMA and phloretin inhibited Li^+ efflux, the planned contrast was statistically significant for k_{out} ($t(35) = 7.01$, one-tailed $P < 0.0001$), and v_{out} ($t(35) = 6.32$, one-tailed $P < 0.0001$), indicating that HMA and phloretin were the only modulators to affect Li^+ efflux significantly as compared to the control condition (Fig. 1B). These results support the conclusion that the Na^+–Li^+ counter transporter provides a major Li^+ efflux pathway. Results for both Li^+ influx and efflux remained statistically significant when we applied a sequentially rejective Bonferroni procedure.

3.2. Comparison of Li^+ transport in the three cell types

With a 50 mmol/L LiCl-containing PBS incubation and at 1–5% cytocrit or hematocrit (Fig. 2), the largest concentrations of $[Li^+]_i$ as determined by AA spectrophotometry were accumulated by lymphoblastoma cells, followed by neuroblastoma cells, and then by RBCs. We used an orthogonal between-group contrast to test this pattern of Li^+ accumulation across the three cell types within each time point (15, 30, 45, and 60 min), specifying *a priori* weights of 1, 0, and −1 for the means of lymphoblastoma, neuroblastoma, and RBCs, respectively. Confirming our hypotheses, the planned contrast was statistically significant at each of the four time points, $t(57) > 12.15$, one-tailed $P < 0.0001$. Thus, the predicted pattern of means for the three cell types, i.e. lymphoblastoma > neuroblastoma > RBC, fitted the data significantly better than expected by chance, collapsing across the four time points.

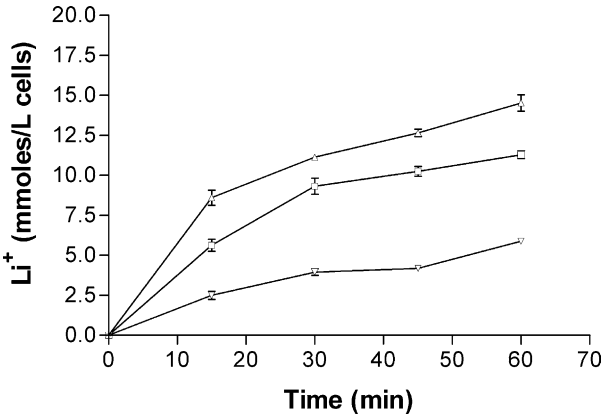

Fig. 2. Intracellular Li^+ accumulation in three cell types. Comparison of $[Li^+]_i$ (in mmoles Li^+/L cells; N = 5) in human lymphoblastoma (△), neuroblastoma (□), and RBCs (▽) in 50 mmol/L LiCl PBS over a 60-min period. Values represent means ± SEM.

3.3. Comparison of Li^+ immobilization and binding in the three cell types

Before performing the Li^+ binding studies, we assessed the cell viability of the agarose-embedded lymphoblastoma cells during the perfusion experiments. In particular, we performed two ^{31}P NMR experiments on lymphoblastoma cells with spectra acquired each hour over a 3 hr period. The NMR chemical shift separation between the resonances of the α- and γ-phosphates of ATP remained fairly constant at 5.1 ppm (Table 1), providing an estimate of intracellular pH of 7.2–7.4 [21]. Additionally, the area ratio of the β-phosphate of ATP over P_i ([β-ATP]/[P_i]), a measure of cellular energy levels [20], remained approximately constant for both experiments (Table 1). At the conclusion of each experiment, we also measured cell viability by using the Trypan blue dye exclusion assay [22] and found it to be above 95% in both trials.

Using $HTmDOTP^{4-}$ to separate the intra- and extracellular ^7Li NMR resonances, we compared the intracellular ^7Li NMR T_1/T_2 ratio at similar $[Li^+]_i$ values (mean ± SD; mmoles Li^+/L cells; N = 3) across lymphoblastoma (3.1 ± 0.3), neuroblastoma (2.9 ± 0.3) [10], and RBCs (3.5 ± 0.4 [26]; Table 2). The large difference between the T_1 and T_2 values for each of the three cell types indicates that Li^+ is highly immobilized within each cell type. To test the hypothesis that the ^7Li T_1/T_2 ratios for Li^+ were higher in neuroblastoma than in lymphoblastoma cells, which were both higher than in RBCs, we used a planned orthogonal between-group contrast, specifying *a priori* weights of 1, 0, and −1 for the means of neuroblastoma cells, lymphoblastoma cells, and RBCs, respectively. Confirming the hypothesized pattern of mean differences, the planned contrast was statistically significant, $t(6) = 16.76$, one-tailed $P < 0.0001$ (Table 2).

Table 1
Cell viability of lymphoblastoma cells during two ^{31}P NMR perfusion experiments by use of the chemical shift ($\delta_{\alpha\gamma}$) and area parameters as probes of the intracellular pH and ATP levels, respectively

Trial	Time (hr)	$\delta_{\alpha\gamma}$ (ppm)	[β-ATP]/[P_i]
1	1	5.07	0.18
	2	5.02	0.20
	3	5.00	0.20
2	1	5.12	0.14
	2	5.05	0.15
	3	5.06	0.17

Table 2
^7Li NMR relaxation values in human lymphoblastoma cells, human neuroblastoma cells, and human RBCs, as well as for their plasma membranes[a]

Sample[b]	$[Li^+]_i$[c]	T_1 (s)	T_2 (s)	T_1/T_2
Lymphoblastoma cells	3.1 ± 0.3	2.6 ± 0.4	0.06 ± 0.01	43 ± 4
Neuroblastoma cells	2.9 ± 0.3	5.1 ± 0.8	0.05 ± 0.02	100 ± 10
RBCs	3.5 ± 0.4	6.5 ± 0.2	0.5 ± 0.01	14 ± 1
Lymphoblastoma PM[d]	4.0	11.5 ± 1.3	0.06 ± 0.01	207 ± 23
Neuroblastoma PM[d]	4.0	12.7 ± 0.9	0.05 ± 0.01	236 ± 73
RBC PM[d]	4.0	12.1 ± 0.5	0.06 ± 0.01	198 ± 33

[a] Means ± SD, N = 3 are presented.
[b] Data represent a compilation of new data and previous work [10,26].
[c] The intracellular Li^+ concentration units are in mmoles Li^+/L of cells.
[d] Protein concentration was 8.0 ± 0.5 mg/mL and viscosity 5.0 ± 0.5 cP.

At 4.0 mmol/L Li^+, the ^7Li T_1/T_2 ratio values of the Li^+-treated PMs for the three cell types were not statistically different, $F(2,6) = 0.50$, $P < 0.64$ (Table 2). To determine the K_{Li} values, we titrated the PM fractions at constant plasma protein concentration (8.0 ± 0.5 mg/mL) with 2–12 mmol/L LiCl and with 500 mmol/L LiCl. The K_{Li} values (in M^{-1}) of the PMs in the lymphoblastoma cells, neuroblastoma cells, and RBCs were 340 ± 53 (N = 4), 340 ± 42 (N = 5), and 185 ± 27 ([26]; N = 5), respectively. To test the hypothesis that PMs from neuroblastoma and lymphoblastoma cells would have equivalent mean K_{Li} values and would both have higher mean K_{Li} values as compared to PMs from RBCs, we used a planned orthogonal between-group contrast, specifying *a priori* weights of 1, 1, and −2 for the means of neuroblastoma cells, lymphoblastoma cells, and RBCs, respectively. Confirming the hypothesized pattern of mean differences, the planned contrast was statistically significant, $t(11) = 6.75$, one-tailed $P < 0.0001$.

3.4. Li^+/Mg^{2+} competition at either similar $[Li^+]_{ex}$ or $[Li^+]_i$

For each cell type, the $[Mg^{2+}]_f$ values (Fig. 3A) and the percentage changes in $[Mg^{2+}]_f$ from the resting $[Mg^{2+}]_f$ values (Fig. 3B) are shown under both *similar* $[Li^+]_{ex}$ or $[Li^+]_i$ conditions. For the similar $[Li^+]_{ex}$ condition, the $[Li^+]_i$ values (in mmoles Li^+/L of cells) after 30 min incubation in 50 mmol/L LiCl-containing PBS, as determined by the AA method (at 1–5% cytocrit for each cell

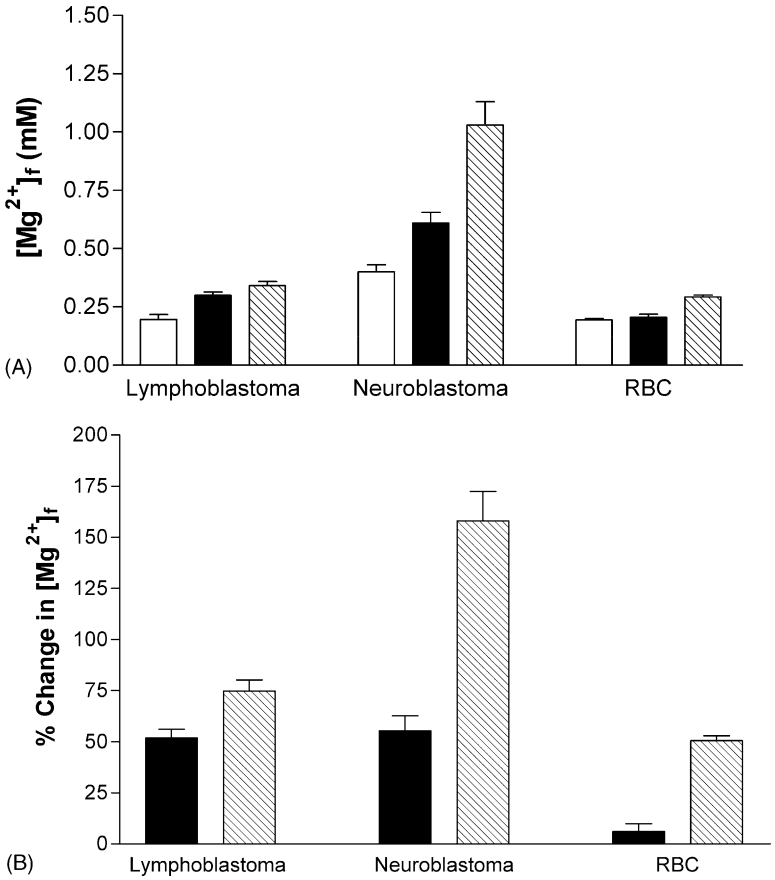

Fig. 3. Effect of Li^+ incubation on free intracellular $[Mg^{2+}]$ in three cell types. $[Mg^{2+}]_f$ (in mmol/L) (A) and percentage increase in $[Mg^{2+}]_f$ from the resting state $[Mg^{2+}]_f$ (B) in human lymphoblastoma cells (N = 3), human neuroblastoma cells ([5]; N = 4), and human RBCs (N = 3) under Li^+-free conditions (white bars, only in Fig. 3A), when the cells were loaded for 30 min in 50 mmol/L LiCl PBS (black bars), and when the $[Li^+]_i$ was approximately 15 mmol/L (striped bars). Values in (A) represent means ± SD and values in (B) represent means ± SEM.

type; N = 5), were 11.1 ± 0.3, 9.3 ± 0.5, and 4.0 ± 0.5 for the lymphoblastoma, neuroblastoma, and RBCs, respectively (Fig. 2; for statistical analysis, see third paragraph of Section 3). For the similar $[Li^+]_i$ condition, the $[Li^+]_i$ values (in mmoles Li^+/L of cells), as determined by AA (at 1–5% cytocrit for each cell type; N = 5), were 14.5 ± 1.2, 15.1 ± 2.3, and 16.6 ± 1.2 for the lymphoblastoma cells, neuroblastoma cells, and RBCs, respectively. ANOVA revealed that these three means were not significantly different from one another, $F(2, 12) = 2.15$, $P < 0.16$.

Because the measured $[Li^+]_i$ values were higher in cells loaded with Li^+ under the similar $[Li^+]_i$ condition than those in cells loaded using the similar $[Li^+]_{ex}$ condition, and cells lacking Li^+ in the Li^+-free condition, we first hypothesized that higher $[Li^+]_i$ values would produce larger increases in the $[Mg^{2+}]_f$ values for each cell type. Therefore, we used between-group orthogonal contrasts to test the hypothesis that the similar $[Li^+]_i$ condition (+1) had a higher $[Mg^{2+}]_f$ value than did the similar $[Li^+]_{ex}$ condition (0), which, in turn, had a higher $[Mg^{2+}]_f$ value than did the Li^+-free condition (−1), collapsing across the three cell types, $t(29) = 2.62$, one-tailed $P < 0.007$ (Fig. 3A), which confirms that the competition is greater in the presence of more $[Li^+]_i$. Also supporting our hypotheses, a between-group orthogonal contrast indicated that the percentage change in $[Mg^{2+}]_f$ was greater for the similar $[Li^+]_i$ condition (+1) than for the similar $[Li^+]_{ex}$ condition (−1), collapsing across the three types of cells, $t(19) = 3.14$, one-tailed $P < 0.003$. For each cell type, this indicates that the competition was greater when more $[Li^+]_i$ was in the cell.

Because the resting state $[Mg^{2+}]_f$ values are different for each cell type (Fig. 3A), it is not appropriate to compare the mean values of $[Mg^{2+}]_f$ of the three types of cells. Therefore, we used the percentage change in $[Mg^{2+}]_f$ when comparing Li^+/Mg^{2+} competition among cell types (Fig. 3B). We hypothesized that, under similar $[Li^+]_{ex}$ conditions, the extent of the Li^+/Mg^{2+} competition will be similar in lymphoblastoma and neuroblastoma cells, and much less in RBCs (Fig. 3B; black bars). Confirming hypotheses, between-group orthogonal contrasts of the percentage change in $[Mg^{2+}]_f$ indicated that neuroblastoma cells (+1) had a similar percentage change in $[Mg^{2+}]_f$ as lymphoblastoma cells (+1); both had higher percentage changes in $[Mg^{2+}]_f$ than did RBCs (−2), collapsing across experimental conditions, $t(8) = 6.35$, one-tailed $P < 0.0001$. In addition, within the similar $[Li^+]_{ex}$ condition, there was no significant difference between neuroblastoma

and lymphoblastoma cells in the percentage change of $[Mg^{2+}]_f$ ($t(6) = 0.41$, two-tailed $P < 0.70$). These data indicate that, under similar $[Li^+]_{ex}$ loading conditions, the extent of the Li^+/Mg^{2+} competition will be similar in lymphoblastoma and neuroblastoma cells, and much less in RBCs.

The percentage changes in $[Mg^{2+}]_f$ for the three cell types after $[Li^+]_i$ reached ~15 mmol/L (striped bars) are shown Fig. 3B. We hypothesized that under similar $[Li^+]_i$ conditions, neuroblastoma cells would show the greatest percentage change in $[Mg^{2+}]_f$ followed by lymphoblastoma cells and the least change in RBCs. Confirming our hypothesis, a between-group orthogonal contrast indicated that neuroblastoma cells (+1) showed a greater percentage change in $[Mg^{2+}]_f$ than did lymphoblastoma cells (0), which, in turn, showed greater percentage changes in $[Mg^{2+}]_f$ than did RBCs (−1), collapsing across experimental conditions, $t(18) = 3.46$, one-tailed $P < 0.002$. The different extent of percentage changes in $[Mg^{2+}]_f$ is likely due to the different degrees of Li^+ immobilization in the three cell types (see Table 2).

For $[Mg^{2+}]_f$ measurements, fluorescence spectroscopy was used with lymphoblastoma and neuroblastoma cells, but the ^{31}P NMR method was used for RBCs, because of the strong intrinsic fluorescence of hemoglobin, which required modified hematocrit conditions (see Section 2). Therefore, we assessed whether the $[Li^+]_i$ values in RBCs were affected during the ^{31}P NMR measurements. For the 50 mmol/L LiCl-containing PBS condition, the $[Li^+]_i$ value (mmoles Li^+/L cells) was determined at 50% hematocrit after the NMR measurement period was completed (30 min) to be 3.9 ± 1.1 (N = 5), which is not significantly different from 4.0 ± 0.5 (N = 5), which was observed after 30 min of incubation at 1–5% hematocrit in 50 mmol/L LiCl-containing PBS, $t(8) = 0.10$, two-tailed $P < 0.93$. For the 150 mmol/L LiCl-containing HBS condition, the mean value of $[Li^+]_i$ (mmoles Li^+/L cells) at 50% hematocrit was 15.1 ± 1.1 (N = 5) after the 30 min NMR measurement period, which is not significantly different from 16.6 ± 1.2 (N = 5), which was observed at 1–5% hematocrit after 60 min in 150 mmol/L LiCl-containing HBS, $t(8) = 2.06$, two-tailed $P < 0.08$.

4. Discussion

4.1. Comparison of Li^+ transport properties

Li^+ transport pathways have been shown to be cell-type specific [10,36,37]. Because ouabain affected Li^+ influx (Fig. 1A), we conclude that Na^+/K^+–ATPase provides a major Li^+ influx pathway in lymphoblastoma cells. In RBCs and excitable cells [36], Na^+/K^+–ATPase was shown not to be a major Li^+ influx path in the presence of physiologic levels of Na^+ and K^+. The major Li^+ influx pathway in RBCs under physiologic conditions is the DIDS-sensitive anion exchange pathway [36]. For the lymphoblastoma transport experiments, there was sufficient carbonate in the growth medium to form a complex with Li^+, which is necessary for transport of Li^+ by the anion exchange pathway [36]. However, this pathway was shown not to be a major influx pathway in lymphoblastoma cells (Fig. 1A) or in neuroblastoma cells [10]. In human neuroblastoma SH-SY5Y cells and other excitable cells, it has been shown that voltage-gated Na^+ channels provide the major contribution to Li^+ influx [10,36]. However, the lymphoblastoma cell line has only low amounts of voltage-gated Na^+ channels [38]. Therefore, as expected, veratridine did not alter Li^+ transport in these cells.

In RBCs, the Na^+/Li^+ countertransport pathway is a major Li^+ efflux pathway [36]. Li^+ efflux in nerve cells is thought to occur via a countertransport mechanism (possibly Na^+/Li^+ countertransport) [36]. With human neuroblastoma cells, phloretin, a Na^+/Li^+ countertransport blocker, did not inhibit Li^+ efflux [10], which may be due to the low specificity of this blocker as compared to the more specific inhibitor, HMA [18]. In our study, both blockers, HMA and phloretin, produced a significant effect by decreasing the Li^+ efflux rates in lymphoblastoma cells, in which HMA produced the largest effect (Fig. 1B). Therefore, Na^+/Li^+ countertransport is the major Li^+ efflux pathway in lymphoblastoma cells and RBCs, and possibly in excitable cells.

Lymphoblastoma and neuroblastoma cells have membrane potentials in the range of −50 to −90 mV [38]. In contrast, RBCs have a membrane potential of −10 mV [36]. Because lymphoblastoma and neuroblastoma cells have similar and larger membrane potentials as compared to RBCs, one would predict that lymphoblastoma and neuroblastoma cells should accumulate much more Li^+ than do RBCs. The accumulation of Li^+ in these cell types partially follows this trend (Fig. 2); however, the variations in Li^+ transport pathways presumably cause further Li^+ accumulation differences in the three cell types.

4.2. Comparison of Li^+ binding and immobilization

In the following discussion, we use the ^7Li NMR T_1/T_2 ratio as a measure of the Li^+ correlation time to address its immobilization and the individual T_1 and T_2 values for Li^+ binding (see Section 2 for interpretation of NMR relaxation measurements and distinction between binding and immobilization). As seen in Table 2, the ^7Li NMR T_1/T_2 ratio is greatest in neuroblastoma cells, less in lymphoblastoma cells, and least in RBCs. This indicates that the correlation time of the Li^+ nuclei and Li^+ immobilization is largest in neuroblastoma cells and smallest in RBCs. Because the ^7Li NMR T_1/T_2 ratios are approximately equal for each PM fraction, Li^+ immobilization is similar among the PM fractions studied. A comparison of the PM fractions to the intact cells in regard to the ^7Li NMR T_1/T_2 ratio is not valid, because the plasma membrane protein concentration

in the intact cells will vary between cell types, and cannot be compared to the PM fractions in which the protein concentration was controlled.

Because the plasma membrane is the major Li^+ binding site in RBCs [26], we explored the possibility that the PM affinities might explain the differences in Li^+ immobilization in the three cell types. Because the observed T_1 and T_2 values were similar in PM suspensions, it is not surprising that the binding constants to the different PMs were also found to be of the same order of magnitude. Therefore, the differences between the intact cells in Li^+ immobilization are hypothesized to be due to Li^+ immobilization to other cell components and not Li^+ immobilization by PMs. Alternatively, this may suggest that more binding sites, or sites with different affinities, exist in the neuroblastoma cells as compared to the other two cell types.

4.3. Comparison of Li^+/Mg^{2+} competition

Under similar $[Li^+]_{ex}$ loading conditions, the percentage change in $[Mg^{2+}]_f$ are approximately equal in lymphoblastoma and neuroblastoma cells, whereas it is much less in RBCs (Fig. 3). Furthermore, the total Li^+ accumulation was greatest in lymphoblastoma cells, followed by neuroblastoma, and then RBCs. Even though lymphoblastoma cells accumulate a larger amount of $[Li^+]_i$, this effect may be canceled out by the greater degree of Li^+ immobilization, and increased competition sites present in neuroblastoma cells. This suggests that the effect of Li^+ on Mg^{2+}-dependent metabolism is more similar in lymphoblastoma and neuroblastoma cells than in RBCs, despite differences in Li^+ transport and immobilization properties. Therefore, we expect that, under pharmacologic conditions, these two cell types would experience a similar extent of Li^+/Mg^{2+} competition.

At a *similar* $[Li^+]_i$ of 15 mmol/L, the neuroblastoma cells displayed a 158% increase in $[Mg^{2+}]_f$, whereas the lymphoblastoma cells displayed a 75% increase in $[Mg^{2+}]_f$, and RBCs an increase of 50% (Fig. 3). The variable extent of Li^+ effects on $[Mg^{2+}]_f$ (neuroblastoma cells > lymphoblastoma cells > RBCs) is likely to be a result of the different degrees of Li^+ immobilization in the three cell types (Table 2).

4.4. Relevance to therapeutic Li^+ levels

It has been previously demonstrated that Li^+/Mg^{2+} competition occurs at therapeutic $[Li^+]_i$ levels (0.8–1.5 mmol/L) in human neuroblastoma SH-SY5Y cells [6]. In particular, it was found that, at an $[Li^+]_i$ of 0.8 mmol/L, the percentage change in $[Mg^{2+}]_f$ was 11%. Changes in $[Mg^{2+}]_f$ of the order of 11% would have a large impact on the many Mg^{2+}-sensitive pathways. This reported change in $[Mg^{2+}]_f$ is small; however, other work using RBC membranes has demonstrated that Li^+ at therapeutic levels will compete with 14–21% of Mg^{2+} binding sites [3], and decreases the initial activation of the α-subunit of the recombinant inhibitory G protein by approximately 50% [8]. Moreover, cytosolic $[Mg^{2+}]_f$ has been demonstrated to be strictly regulated in cellular systems since large increases result in neurotoxicity and apoptosis [7,39], while micromolar fluctuations affect the activity of some ion channels [40]. From extrapolation of our data (Fig. 3), we used the proportional relationship {percentage change in $[Mg^{2+}]_f$}/$[Li^+]_i$ to calculate the percentage change of $[Mg^{2+}]_f$ at 0.8 mM $[Li^+]_i$ and found that there was a 3.7–4.1% and 1.2–2.4% change for lymphoblastoma and RBCs, respectively. Based on these calculations, it is apparent that it would be difficult to observe this competition at therapeutic $[Li^+]_i$ levels for every cell type. At therapeutic $[Li^+]_i$ levels, the extent of Li^+/Mg^{2+} competition will be different in various cell types and can be predicted from the transport, immobilization, and binding properties of Li^+. Li^+/Mg^{2+} competition will increase with increased immobilization, binding, and accumulation of $[Li^+]_i$.

With the recent advances in ^7Li magnetic resonance imaging (MRI) techniques, Li^+ levels and binding parameters (T_1 and T_2) can be measured within various locations in the brain [41,42]. It should be possible to predict locations in the body and brain where the greatest effect of Li^+ on Mg^{2+}-dependent metabolism will be observed. Furthermore, the use of ^{31}P MRI methods for measuring localized $[Mg^{2+}]_f$ should complement these studies [43]. In summary, the effects of Li^+ on Mg^{2+}-dependent enzymes can be better understood with a knowledge of the extent of the ionic competition mechanism in particular cell types.

Acknowledgments

Financial support from NIMH (grant number MH-45926) to D.M. de F., from NSF-REU Training Grant (CHE-9619709) to L.C., from FCT, Portugal (grant POCTI/1999/36160) to C.F.G.C.G. and M.M.C.A.C., and Praxis (XXI/BD/21462/99) to C.P.F. is acknowledged.

References

[1] Birch NJ. Letter: lithium and magnesium-dependent enzymes. Lancet 1974;2:965–6.

[2] Amari L, Layden B, Rong Q, Geraldes CFGC, Mota de Freitas D. Comparison of fluorescence ^{31}P NMR and ^7Li NMR spectroscopic methods for investigating Li^+/Mg^{2+} competition for biomolecules. Anal Biochem 1999;272:1–7.

[3] Mota de Freitas D, Amari L, Srinivasan C, Rong Q, Ramasamy R, Abraha A, Geraldes CF, Boyd MK. Competition between Li^+ and Mg^{2+} for the phosphate groups in the human erythrocyte membrane and ATP: an NMR and fluorescence study. Biochemistry 1994;33:4101–10.

[4] Ramasamy R, Mota de Freitas D. Competition between Li^+ and Mg^{2+} for ATP in human erythrocytes. A ^{31}P NMR and optical spectroscopy study. FEBS Lett 1989;244:223–6.

[5] Amari L, Layden B, Nikolakopoulos J, Rong Q, Mota de Freitas D, Baltazar G, Castro MMCA, Geraldes CFGC. Competition between Li^+ and Mg^{2+} in neuroblastoma SH-SY5Y cells: a fluorescence and ^{31}P NMR study. Biophys J 1999;76:2934–42.
[6] Abukhdeir AM, Layden BT, Minadeo N, Bryant FB, Stubbs EB, Mota de Freitas D. Effect of chronic Li^+ treatment on free intracellular Mg^{2+} in human neuroblastoma SH-SY5Y cells. Bipolar Disord 2003;5:6–13.
[7] Cheng C, Reynolds IJ. Subcellular localization of glutamate-stimulated intracellular magnesium concentration changes in cultured rat forebrain neurons using confocal microscopy. Neuroscience 2000; 95:973–9.
[8] Minadeo N, Layden B, Amari LV, Thomas V, Radloff K, Srinivasan C, Hamm HE, Mota de Freitas D. Effect of Li^+ upon the Mg^{2+}-dependent activation of recombinant $G_{i\alpha 1}$. Arch Biochem Biophys 2001;388: 7–12.
[9] Avissar S, Schreiber G, Danon A, Belmaker RH. Lithium inhibits adrenergic and cholinergic increases in GTP binding in rat cortex. Nature 1988;331:440–2.
[10] Nikolakopoulos J, Zachariah C, Mota de Freitas D, Ramasamy R, Castro MMCA, Geraldes CFGC. ^7Li nuclear magnetic resonance study for the determination of Li^+ properties in neuroblastoma SH-SY5Y cells. J Neurochem 1998;71:1676–83.
[11] Allison JH, Stewart MA. Reduced brain inositol in lithium-treated rats. Nature 1971;233:267–8.
[12] Grimes CA, Jope RS. CREB DNA binding activity is inhibited by glycogen synthase kinase-3β and facilitated by lithium. J Neurochem 2001;78:1219–32.
[13] Jope RS. Anti-bipolar therapy: mechanism of action of lithium. Mol Psychiatry 1999;4:117–28.
[14] Ryves WJ, Harwood AJ. Lithium inhibits glycogen synthase kinase-3 by competition for magnesium. Biochem Biophys Res Commun 2001;280:720–5.
[15] Ebstein R, Belmaker R, Grunhaus L, Rimon R. Lithium inhibition of adrenaline-stimulated adenylate cyclase in humans. Nature 1976;259: 411–3.
[16] Goldberg H, Clayman P, Skorecki K. Mechanism of Li inhibition of vasopressin-sensitive adenylate cyclase in cultured renal epithelial cells. Am J Physiol 1988;255:F995–F1002.
[17] Lazarus JH. Endocrine and Metabolic Effects of Lithium. New York: Plenum Medical Book Company; 1986.
[18] Chi Y, Mo S, Mota de Freitas D. Na^+–H^+ and Na^+–Li^+ exchange are mediated by the same membrane transport protein in human red blood cells: an NMR investigation. Biochemistry 1996;35:12433–42.
[19] Layden B, Diven C, Minadeo N, Bryant FB, Mota de Freitas D. Li^+/Mg^{2+} competition at therapeutic intracellular Li^+ levels in human neuroblastoma SH-SY5Y cells. Bipolar Disord 2000;2:200–4.
[20] Kaplan O, Aebersold P, Cohen JS. Metabolism of peripheral lymphocytes, interleukin-2-activated lymphocytes and tumor-infiltrating lymphocytes from ^{31}P NMR studies. FEBS Lett 1989;258:55–8.
[21] Gadian DG. NMR and its Applications to Living Systems. Oxford: Oxford Press; 1995.
[22] Patterson Jr MK. Measurement of growth and viability of cells in culture. Methods Enzymol 1979;58:141–52.
[23] Pauly T, Dahmen N, Szegedi A, Wetzel H, Bol GF, Ferdinand K, Hiemke C. Blood ethanol levels and adenylyl cyclase activity in lymphocytes of alcoholic patients. Biol Psychiatry 1999;45: 489–93.
[24] Costa EM, Hoffmann BB, Loew GH. Opioid agonists binding and responses in SH-SY5Y cells. Life Sci 1992;50:73–81.
[25] Srinivasan C, Minadeo N, Toon J, Graham D, Mota de Freitas D, Geraldes CFGC. Competition between Na^+ and Li^+ for unsealed and cytoskeleton-depleted human red blood cell membrane: a ^{23}Na multiple quantum filtered and ^7Li NMR relaxation study. J Magn Reson 1999;140:206–17.
[26] Rong Q, Espanol MCT, Mota de Freitas D, Geraldes CFGC. ^7Li NMR relaxation study of Li^+ binding in human erythrocytes. Biochemistry 1993;32:13490–8.
[27] Lin W, Mota de Freitas D, Zhang Q, Olsen KW. Nuclear magnetic resonance and oxygen affinity study of cesium binding in human erythrocytes. Arch Biochem Biophys 1999;369:78–88.
[28] Fanger BO. Adaptation of the Bradford protein assay to membrane-bound proteins by solubilizing in glucopyranoside detergents. Anal Biochem 1987;162:11–7.
[29] James TL, Noggle JH. ^{23}Na nuclear magnetic resonance relaxation studies of sodium ion interaction with soluble RNA. Proc Natl Acad Sci USA 1969;62:644–9.
[30] Howarth O. Relaxation and Related Time-Dependent Processes. In: Mason J, editor. Multinuclear NMR. New York: Plenum Press; 1987.
[31] Hubbard PS. Nonexponential nuclear magnetic relaxation by quadrupole interactions. J Chem Phys 1970;53:985–7.
[32] Rubinstein M, Baram A, Luz Z. Electronic and nuclear relaxation in solutions of transition metal ions with spin $S = 3/2$ and 5/2. Mol Phys 1971;20:67–80.
[33] Reuben J, Luz Z. Longitudinal relaxation in spin 7/2 systems. Frequency dependence of lanthanum-139 relaxation times in protein solutions as a method of studying macromolecular dynamics. J Phys Chem 1976;80:1357–61.
[34] Rosenthal R, Rubin DB, Rosnow RL. Contrasts and effect sizes in behavioral research: a correlational approach. Cambridge: Cambridge University Press; 2000.
[35] Holland BS, Copenhaver MD. An improved sequentially rejective Bonferroni test procedure. Biometrics 1987;43:417–23.
[36] Ehrlich BE, Diamond JM. Lithium, membranes and manic-depressive illness. J Membr Biol 1980;52:187–200.
[37] Duhm J. Pathways of Lithium Transport Across the Human Erythrocyte Membrane. In: Thellier M, Wissocq J-C, editors. Lithium Kinetics. Lancashire: Marius Press; 1992. p. 27–53.
[38] DeCoursey TE, Chandy KG, Gupta S, Cahalan MD. Voltage-dependent ion channels in T-lymphocytes. J Neuroimmunol 1985;10:71–95.
[39] Hartnett KA, Stout AK, Rajdev S, Rosenberg PA, Reynolds IJ, Aizenman E. NMDA receptor-mediated neurotoxicity: a paradoxical requirement for extracellular Mg^{2+} in Na^+/Ca^{2+}-free solutions in rat cortical neurons *in vitro*. J Neurochem 1997;68:1836–45.
[40] Jung DW, Brierley GP. Matrix free Mg^{2+} and the regulation of mitochondrial volume. Am J Physiol 1999;277:C1194–201.
[41] González RG, Guimaraes AR, Sachs GS, Rosenbaum JF, Garwood M, Renshaw PF. Measurement of human brain lithium *in vivo* by MR spectroscopy. Am J Neuroradiol 1993;14:1027–37.
[42] Komoroski RA, Pearce JM, Newton JE. The distribution of lithium in rat brain and muscle *in vivo* by ^7Li NMR imaging. Magn Reson Med 1997;38:275–8.
[43] Hugg JW, Matson GB, Twieg DB, Maudsley AA, Sappey-Marinier D, Weiner MW. Phosphorus-31 MR spectroscopic imaging (MRSI) of normal and pathological human brains. Magn Reson Imaging 1992; 10:227–43.